RSC Advances

PAPER

Cite this: *RSC Adv.*, 2014, **4**, 48458

# Electro-catalytically active Au@Pt nanoparticles for hydrogen evolution reaction: an insight into a tryptophan mediated supramolecular interface towards a universal core–shell synthesis approach†

Sarvesh Kumar Srivastava,[a] Jonathan Sabaté del Río,[b] Ciara K. O'Sullivan,[bc] Chiaki Ogino[a] and Akihiko Kondo*[a]

We report an eco-friendly, one-pot, room-temperature method for the rapid synthesis of electrocatalytically active Au@Pt (50 nm) bimetallic nanoparticles *via* a tryptophan (Trp) mediated supramolecular interface in an aqueous environment. Our results demonstrate a simple universal approach for high shell–metal loading where a pre-stabilized tryptophan polymerized-Au core serves as a template to facilitate subsequent deposition of Pt. We observed that the amine-stabilized poly-Trp bi-layer has an enhancing effect on the electrocatalytic potential of Au@Pt NPs by the virtue of an amine stabilized interface, thereby enhancing the HER activity over glassy carbon electrodes. Several characterization techniques were used to confirm the inherent core–shell morphology of the resulting Au@Pt NPs. This Trp mediated facile green synthesis strategy has the potential to synthesize an array of Au-core containing bimetallic nanoparticles with enhanced catalytic activity and stable structure integration.

Received 8th August 2014
Accepted 19th September 2014

DOI: 10.1039/c4ra08365b

www.rsc.org/advances

## Introduction

Bimetallic nanoparticles (NPs) have gained tremendous importance due to their composition-dependent optical, catalytic and magnetic properties, which are markedly different to those of their monometallic counterparts.[1,2] Au@Pt core–shell structures in particular, have garnered enormous interest for use in catalysis and fuel cell technology due to their unique hybrid structure that facilitates greater synergistic potential and stability.[3,4] Galvanic replacement[5] is a commonly used technique for the synthesis of core–shell structures where one metal layer is electrochemically deposited over the surface of another *via* application of a potential difference, inherently making the process energy intensive with marked difficulty in achieving monolayer Pt deposition over the Au shell. To overcome this problem, the so-called Under Potential Deposition (UPD)[6] technique has been reported where a layer of copper is preformed for subsequent deposition of the Pt shell. However, UPD is not feasible for the mass production of these particles as it is difficult to achieve the layer dynamics, and several techniques have thus evolved utilizing surface adsorbents and polymers to achieve core–shell morphology.[7,8] Although, these techniques do offer an alternative synthesis approach, most of them still require toxic solvents/chemicals, intensive process control and suffer from the formation of an unstable 'bi-layer binder' under electrocatalytic conditions. There is thus a mature need to produce these valuable core–shell structures in a more facile and eco-friendly manner without compromising their catalytic properties.

Biogenic synthesis of nanomaterials promises to deliver a sustainable, environmentally-friendly method of producing advanced nanomaterials with novel properties *via* exploitation of naturally occurring compounds.[9–11] These green nanomaterials not only compete with current techniques in terms of mass-production and reduction of costs, but can also result in enhanced loading of metal nanoparticles, a grand challenge that is of particular interest for fuel cells.[12,13] Biogenic nanomaterials evolving from phytochemicals, microbes/cells as well as biomolecules including lipids, proteins and amino acids *etc.* have been harnessed to supply the ever-growing need for sustainable nanomaterials ranging from monometallic nanoparticles,[14,15] surface-modified carbonaceous substrates[16] and bimetallic nanoparticles[17] *etc.*

[a]*Department of Chemical Science and Engineering, Graduate School of Engineering, Kobe University, 1-1 Rokkodai-cho, Nada, Kobe, 657-8501, Japan. E-mail: akondo@kobe-u.ac.jp; Fax: +81-78-803-6196; Tel: +81-78-803-6196*

[b]*Nanobiotechnology & Bioanalysis Group, Department of Chemical Engineering, Universitat Rovira i Virgili, Avinguda Països Catalans, 26, Tarragona 43007, Spain. E-mail: ciara.osullivan@urv.cat; Tel: +34-9775-5840*

[c]*ICREA, Passeig Lluis Companys 23, 08010 Barcelona, Spain*

† Electronic supplementary information (ESI) available: XPS data of Au@Pt NPs. CV behaviour of free tryptophan. Preliminary UV-Vis data and HR-TEM images for Au@Ag and Au@Rh NPs. See DOI: 10.1039/c4ra08365b

Amino compounds including amino acids have shown promise for use as effective reducing agents for the preparation of monometallic nanoparticles.[18,19] Recently, we reported Au@Pd core–shell nanoparticle synthesis *via* a tryptophan (Trp) mediated supramolecular interface[20] where we observed that Trp plays an important role in core–shell structure formation *via* synthesis of monometallic nanoparticles (Au) through oxidation of the amino acid, which in turn forms a poly-Trp layer that caps and stabilizes the resulting shell-layer (Pd) resulting in Au@Pd nanoparticles.[21,22] Furthermore, we observed the inherent amide linkages not only resulted in stable core–shell structures but also enhanced the overall catalytic activity most likely due to anion distribution *via* N-doping of amide linkages.[23] In the work reported here, we extend the application of this core–shell nanoparticle synthesis protocol to achieve room temperature synthesis of Au@Pt NPs and their subsequent application in the electro-oxidation of water. Gold seeds (Au NPs) were produced by incorporating tryptophan in the aqueous reaction mixture followed by successive reduction of Pt ions over the Au NP surface resulting in core–shell morphology. The resulting nanoparticles were characterized using UV-Vis spectroscopy, transmission electron microscopy (TEM), aberration-corrected high angle annular dark field scanning transmission electron microscopy (AC-HAADF-STEM), energy dispersive X-ray (EDX) elemental mapping and line scanning analysis, X-ray diffraction (XRD) and cyclic voltammetry (CV). Finally, the catalytic properties of the resulting Au, Pt and Au@Pt nanoparticles were demonstrated using hydrogen evolution from water as a model system.

## Experimental section

### (a) Synthesis of Au, Pt and Au@Pt nanoparticles

Chloroauric acid ($HAuCl_4$) and potassium tetrachloroplatinate ($K_2PtCl_4$) were obtained from Scharlau Chemie (Spain) and were used without any pre-treatment. L-Tryptophan was obtained from Naclalai Tesque (Kyoto, Japan). Ultrapure water (18.2 MΩ cm) produced with a Milli-Q RG system (Millipore Ibérica, Spain) was used in all experiments.

Well-mixed gold cation stock solution at 0.5 mM (10 mL) and platinum cation stock solution (0.5 mM, 10 mL) were prepared. Trp aqueous stock solution was prepared at a concentration of 1 mM (20 mL). Cation solutions consisting of Au : Pt was used in the volumetric ratio of 1 : 1.

Gold nanoparticles were then prepared by spontaneous reduction of 10 mL gold cation in the presence of 2 mL of Trp solution with vigorous stirring for 2 hours followed by intermittent sonication for 30 seconds every 15 min. It should be noted that the size of the resulting core–shell structure can be tuned by controlling the size of the Au NPs at the seeding stage. For Au@Pt core–shell NPs, platinum precursor solution (5 mL) was introduced into the gold NP seed solution (5 mL) along with 1 mL of Trp solution. Again, the resulting mixture was stirred for 2 hours followed by intermittent sonication for 10 seconds every 30 minutes. The Pt NP solution was prepared in the same way as mentioned above for Au NP seed synthesis. In this manner, three distinct types of nanoparticles were synthesized – namely Au NPs, Pt NPs and Au@Pt NPs.

### (b) Characterization of Au, Pt and Au@Pt nanoparticles

UV-Visible spectra were obtained using a CARY 100 Bio UV-Vis Spectrophotometer and were analyzed using Varian's Cary Win UV Scan ver. 3.00 (182) software. Nanoparticle formation was monitored from 200–800 nm at a scan rate of 2000 nm $min^{-1}$. The focus of this study was to monitor localized surface plasmon resonance (LSPR) and associated progress of the reaction in the visible region of Au NPs at 540 nm. Morphology and grain size analysis of the resulting Au@Pt NPs was carried out using a JEOL 1011 transmission electron microscope operated at 80 keV with an ultrahigh-resolution pole piece providing a point resolution of 2 Å. Individual Au@Pt nanoparticles were subsequently analyzed by AC-HAADF-STEM (JEOL 2100F, 200 kV, ~0.1 nm point resolution) to observe the precise structure of the resulting core–shell morphology. One micro-liter was taken from the reaction mixtures, placed on carbon coated copper grids and dried at room temperature. The images were analyzed using ImageJ 1.43M software as well as by JED-2300T STEM-EDX to obtain the composition architecture. X-Ray Diffraction (XRD) measurements were made using a Siemens D5000 diffractometer (Bragg–Brentano parafocusing geometry and vertical $\theta$–$\theta$ goniometer) fitted with a curved graphite diffracted-beam monochromator and diffracted-beam Soller slits, a 0.06° receiving slit and scintillation counter as a detector. The angular $2\theta$ diffraction range was between 25 and 100°. A drop of the sample (100 μL) was deposited on to a low background Si (510) sample holder. The data were collected with an angular step of 0.05° at 12 s per step and sample rotation. Cukα radiation was obtained from a copper X-ray tube operated at 40 kV and 30 mA. The chemical nature of metallic nanoparticles were analyzed with Diffracplus Evaluation software (Bruker 2007), which compared the XRD diffractograms with the ICDD data base.

### (c) Preparation of working electrodes

Au NP, Pt NP, and Au@Pt NP mixture solutions were mixed and centrifuged twice with 2 mL acetone–$H_2O$ (1 : 1 v/v) followed by removal of the supernatant in order to eliminate the excess of Trp and other organic moieties adhering to the shell surface. 25 μL of each sample was loaded on the surface of the glassy carbon electrode (GCE) by drop casting under a hot-air flow until completely dried.

### (d) Electrochemical characterization of Au, Pt and Au@Pt nanoparticles

All electrochemical measurements were performed with a potentiostat/galvanostat PGSTAT 12 Autolab controlled by the General Purpose Electrochemical Software (GPES). A three-electrode setup was used with a GCE as working electrode ($\phi$ = 0.126 $cm^2$), a Pt wire as counter electrode and Ag/AgCl electrode with 3 M KCl internal solution (Dri-Ref™-L) as a reference electrode. Before the measurements, the electrochemical cell was purged with $N_2$ gas for 10 minutes. The

characterization of the core–shell NP morphology was realized by diluting the different NP pellets in 20 μL of 0.5 M $H_2SO_4$. This solution was electrochemically characterized by CV analysis in a potential window between −0.2 V and 1.6 V *vs.* Ag/AgCl at a scan rate of 0.1 V $s^{-1}$. Au NP, Pt NP, and Au@Pt NP mixture solutions were washed as described above. The electrocatalytic properties of Au@Pt NPs deposited on the surface of the GCE were examined for the HER (Hydrogen Evolution Reaction) in basic medium.[24,25] The NP-modified GCE were characterized using CV in a potential window between 0 V and −2.0 V *vs.* Ag/AgCl at a scan rate of 10 mV $s^{-1}$ applying[25] consecutive cycles in 90 mM Tris–HCl buffer, pH 8.0, until a steady state was reached in order to check the electrode stability, but only the first cathodic scan was used for analysis.

## Results and discussion

The two general techniques used for the synthesis of core–shell nanoparticles include simultaneous reduction and successive reduction, where the former approach provides better shape control and atomic ratio as compared to the latter, particularly with respect to core–shell structures. To this end, we utilized the successive reduction approach to yield Au@Pt core–shell NPs. The synthesis strategy used has three steps as depicted in Fig. 1. Firstly, Au core nanoparticles were formed and stabilized *via* poly-Trp layer due to the indole group H-bonded supramolecular functionality.[26,27] Next, the shell metal ions (Pt) were introduced into the aqueous reaction mixture, associating with the core ligands *via* the Trp induced supramolecular interface and resulting in the sequestering of Pt(II) onto the surface of Au core *via* active carboxyl groups. Finally, the surface bound Pt(II) was reduced over the Au core, yielding characteristic core–shell structures.

UV-Vis absorbance spectra of Trp synthesized Au@Pt nanoparticles are depicted with reference to Au NP seed formation and subsequent Pt shell loading around the core. Au NP spectra showed an increasing LSPR centred at *ca.* 540 nm (Fig. 2a), and a gradual increase in LSPR was observed to become stabilized

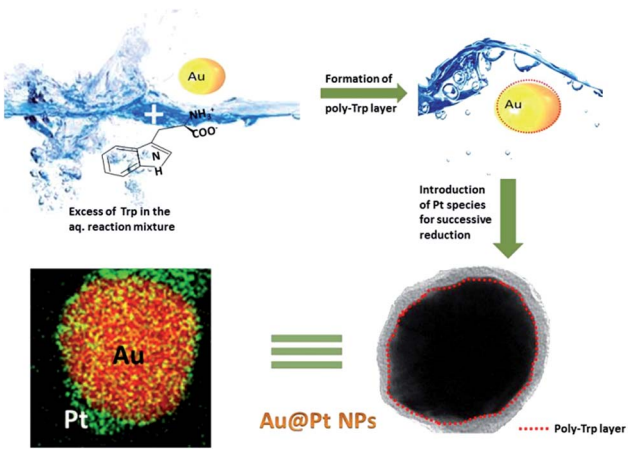


Fig. 1 Schematic representation of tryptophan mediated synthesis of Au@Pt core–shell structure.

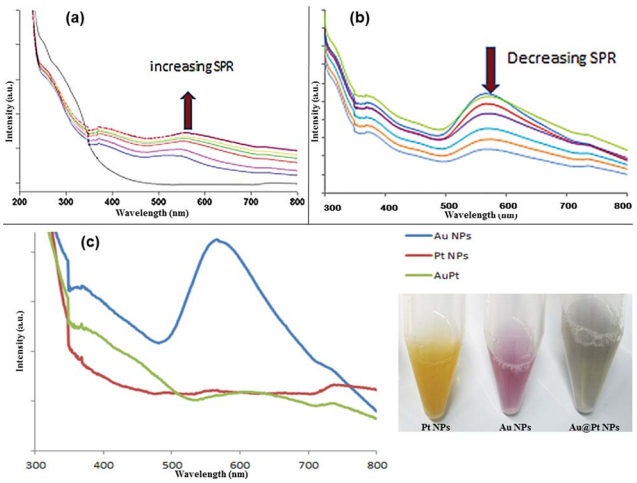


Fig. 2 Growth characteristics in terms of LSPR in (a) formation of Au NPs; (b) deposition of Pt shell over Au NPs; (c) difference in LSPR following completion of reaction (inset: showing visible color difference between all three nanoparticle reaction mixtures).

over a time period of 120 minutes indicating completion of Au NP formation. These Au NPs then acted as the seed for subsequent Pt shell formation resulting in a marked decrease in absorbance at 540 nm over a period of time, as highlighted in Fig. 2b. This also demonstrated that the Pt shell thickness can be controlled by the reaction time while keeping the other reaction parameters constant.

Subsequently, the absorbance spectra of Au, Pt and Au@Pt NPs across the visible region following completion of the reaction were measured as shown in Fig. 2c. It was observed that the absorbance band was drastically reduced in case of Au@Pt NPs and was completely absent in the case of Pt NPs reaction mixture following the completion of reaction.

The change in the dielectric that surrounds the gold combined with the large scattering by the Pt shell may be factors strongly contributing to the loss of SPR.[28] This spectral behaviour indicates the formation of core–shell structure as the surface electron density in the core (Au) increases at the expense of electrons from the outer Pt shell[29] due to the fact that Pt has a higher work function (5.65 eV) than Au (5.10 eV), and the Pt shell coating onto the Au core resulted in gradual dampening of the plasmon of the Au core. Following completion of the reaction, Au NPs were of a pink color due to their characteristic SPR. However, upon Pt loading, the pink hue disappeared and a characteristic grey-black dispersion appeared, indicative of the formation of a thin Pt shell over the Au core (Fig. 2c).

To confirm and characterize the formation of Au@Pt NPs in aqueous solution, TEM followed by high resolution STEM and scattered area electron diffraction (SAED) was carried out (Fig. 3).

TEM imaging confirmed Au@Pt core–shell nanoparticles of *ca.* 50 nm (Fig. 3a), with a truncated polygonal Au core of *ca.* 50 nm and a spongelike-Pt shell of *ca.* 2–8 nm thickness (Fig. 3b). Aberration-corrected high-angle annular dark-field scanning TEM (AC-HAADF-STEM) was used to confirm the core–shell

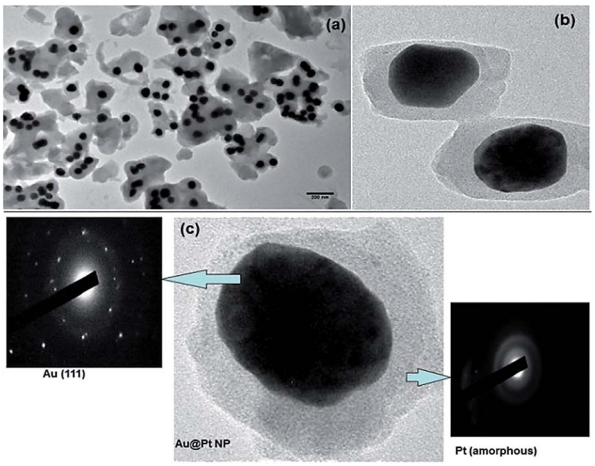


Fig. 3 TEM images showing (a) Au@Pt NP particles; (b) discrete Au@Pt NP particles with core size ~50 nm and shell ~5 nm; (c) HAADF-STEM image of resulting Au@Pt NP showing crystalline Au (111) core and largely amorphous Pt shell.

morphology of the observed Au@Pt NPs. A highly discrete Au@Pt boundary layer was also observed where the Au core in the center showed a diffraction pattern (SAED) characteristic for a Au (111) crystal lattice (Fig. 3c). Additionally, in the absence of any distinct diffraction pattern, the spongelike-Pt shell was rather amorphous in nature. The Au@Pt NPs observed in this study largely comprised of a crystalline Au core with an amorphous Pt shell, which was also confirmed by subsequent XRD analysis (Fig. 4).

As can be seen in Fig. 4, the truncated octahedron Au NP seeds showed a very strong Bragg's diffraction at (111) at 38.2° followed by a weak diffraction at 44.3° which can be assigned to the (200) crystal plane. In the case of Au@Pt NPs, a distinct peak was observed at 77.5° suggesting Au (311) crystal re-arrangement normally observed in core–shell structures. Finally, no credible peaks can be assigned to Pt region as observed in the case of Pt NPs and Au@Pt NPs, thus confirming that the majority of reduced platinum was amorphous in nature. This can be attributed to the fact that the reductive reaction under the supramolecular effect of Trp is rather quick and therefore, resulting Pt atoms are produced rapidly at room temperature where Pt atoms adhere to particles without relaxation/surface tension to balance sites, thereby producing a disordered structure *i.e.* the amorphous state of platinum shell.

Subsequent HAADF-STEM imaging of Au@Pt NPs displayed a brighter gold core due to its' heavier atomic weight whereas the platinum shell appeared comparatively less bright attributable to its low atomic weight (Fig. 5a).

EDX elemental mapping showed that Au atoms (red) and Pt atoms (green) were discretely distributed with a dense Au core at the centre and Pt at the boundary, giving rise to a characteristic core–shell structure (Fig. 5b).

EDX elemental line scanning (Fig. 5c) on single particles confirmed that the Au@Pt NPs were composed of a distinct Au rich centre with an absence of any Pt peaks, which were rather at the boundary, typical of core–shell rather than an alloyed morphology.[30] Following synthesis and characterization of the Au@Pt NPs, their electrocatalytic efficiency was tested. It should be noted that core–shell structures are capable of generating new electrocatalytic properties *via* interaction between the shell (Pt) and underlying core metal (Au) as well as geometrical structures of the Pt including monolayer, island and intermixing phase. Furthermore, contrary to the common belief that only monolayer crystalline structures can have a higher catalytic potential, thin amorphous platinum films are highly desirable end-products sought for application in electrode preparation and electro-oxidation reactions.[31] Moreover, Pt based bimetallic systems for electrochemical reactions have been demonstrated to show that qualitative changes in the surface properties that take place during the deposition of a catalytically active component and the amorphous Pt shell may offer higher catalytic activity (synergistic effect) and selectivity for specific reactions.[32] Amine-stabilized cetyltrimethylammonium chloride (CTAC) has been reported as both a reducing and stabilizing agent in the synthesis of Au@Pd core–shell nanoparticles.[33] Similarly, in our study, Trp plays a key role in the reduction and subsequent stabilization of the core–shell structure *via* amine-carboxyl interphase (ESI†). It can be postulated that the amine-stabilized poly-Trp layer holding the core–shell structure together may also enhance the electrocatalytic potential of Au@Pt NPs, which is supported by previously reported studies that showed amine stabilized substrates to result in the formation of $H_2O$–$NH_4^+$, thereby enhancing HER.[34]

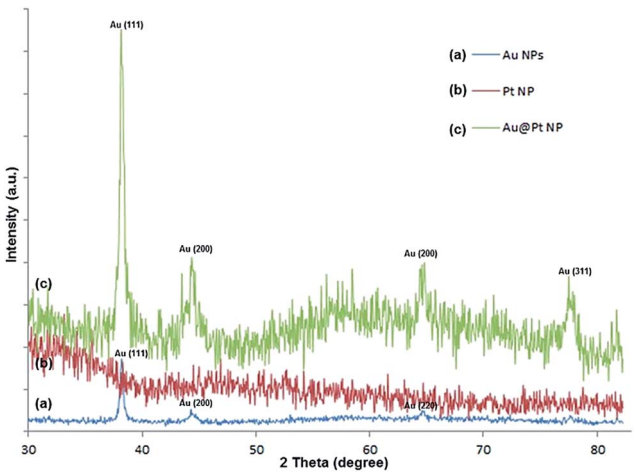


Fig. 4 Showing XRD pattern of Au NPs, Pt NPs and Au@Pt NPs.

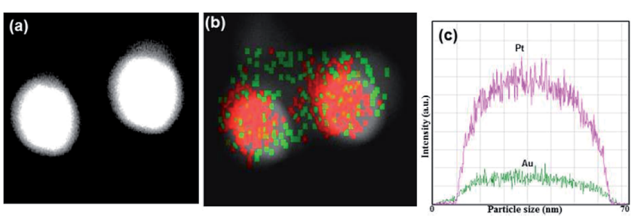


Fig. 5 Showing Au@Pt NPs as observed by (a) AC-HAADF-STEM image; (b) STEM-EDX elemental mapping; (c) line scan EDX.

To explore the electrocatalytic potential of the formed core–shell nanoparticles, cyclic voltammetry was carried out to analyse the Au@Pt surface (Fig. 6). The presence of gold (exposed surface in case of Au@Pt NP) can be electrochemically detected due to its' characteristic peaks (anodic at 0.965 V and cathodic at 0.175 V) when the metal is oxidized or reduced over the boundaries of the electrode as in case of Au NPs coated over GCE. However, no such peaks were observed in the case of Au@Pt NPs and control mixtures (Pt NPs and GCE) thereby indicating that no exposed Au surface was present on the Au@Pt matrix deposited over the electrode surface, and furthermore demonstrates that the underlying polymeric-Trp-layer is stable under the applied electrochemical conditions.

Finally, the electrocatalytic activity of the resulting Au@Pt NPs was tested for the electrochemical oxidation of water (hydrolysis) *via* experimental determination of the potential range where the HER occurs. Three different control electrodes of Au NP coated GCE, Pt NP coated GCE and unfunctionalised GCE were also evaluated to compare to the deposited core–shell structure (Au@Pt). It is widely established that the hydrogen evolution reaction (HER) can be studied by constructing polarization curves on different cathode.[35] Fig. 7 show the polarization curves for the NPs and controls, where different HER potentials are determined by the extrapolation to the region where hydrogen evolution occurs.

We observed that Au@Pt coated GCE significantly decreases the overpotential required to produce HER as compared to regular Pt NPs, also attaining the best performance in terms of current density. Au@Pt NPs facilitated evolution of hydrogen at a voltage as low as −0.86 V *vs.* Ag/AgCl, reaching a maximum current density of −5.98 mA $cm^{-2}$ at −2 V *vs.* Ag/AgCl, whereas Au and Pt NPs only showed electro-oxidation of water at applied voltages of −1.30 V and −1.08 V *vs.* Ag/AgCl, respectively. Although, highest current densities were observed at −2 V, efficiency under these conditions in terms of current density per volt applied tends to decrease due to $H_2$ generation and bubble formation over the electrode surface, thereby reducing the electrolysis area. These experimental results are consistent with the work of Desic *et al.*[36] where 3D-platinum overlayers deposited on gold by acid CV increased the activity of HER as compared with pure gold, platinum or 2D-overlayers of gold deposited on platinum. It has also been reported that the effect of the Pt metallic thickness on gold plays an important role on the efficiency of the HER,[37,38] and the use of Au@Pt with a Pt layer of ∼5 nm as reported here is in agreement with this previously reported work.

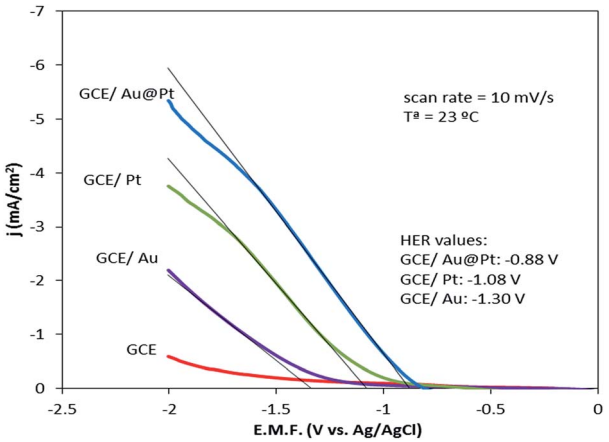


Fig. 7 Polarization curves for the hydrogen evolution reaction on GCE, Au NPs, Pt NPs and Au@Pt NPs between 0 V and −2 V *vs.* Ag/AgCl at a scan rate of 10 mV $s^{-1}$ in 90 mM Tris–HCl buffer, pH 8.0.

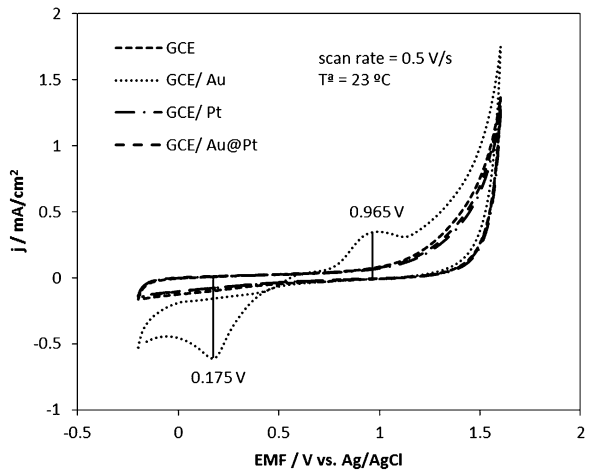


Fig. 6 CV characterization of Au, Pt, Au@Pt NPs and GCE (control) between 1.6 V and −0.2 V *vs.* Ag/AgCl at a scan rate of 0.5 V $s^{-1}$ in $H_2SO_4$ 0.5 M.

Electrocatalytic evaluation was carried out using Tafel analysis,[39] from which the logarithm of the charge transfer (current density) as a function of the applied potential can be used to determine the transfer coefficient (slope) and the exchange current density (intercept). Tafel plots show a linear correlation between the activation overpotential and the logarithmic value of current generated during operation in the region where the HER occurs, from which the determination of lower slopes along with higher exchange current densities signifies a lower charge transfer resistivity. In order to measure the relative cathodic electrochemical activity of the nanoparticles used in this study, the Tafel plot was represented for the HER (Fig. 8), plotting the current densities ($j$) calculated from the polarization curves recorded at 10 mV $s^{-1}$ (Fig. 7) as a function of the applied potential. It should be noted that almost no change was observed with the CV behaviour of free Trp under given reaction conditions.

Fig. 8 shows the Tafel slope for each working electrode on the linear region and the intercept represents the exchange current density ($j_0$), and depending on the fitting method, values of the Tafel slope between *ca.* 50 and 150 mV $decade^{-1}$ can be obtained.[40]

Au@Pt NP coated GCE had a Tafel slope of −39 mV $decade^{-1}$, similar to the value of −35 mV $decade^{-1}$ obtained with the Pt NP coated GCE, whilst the Au@Pt core–shell displayed a higher exchange current density of $2.3 \times 10^{-3}$ A $cm^{-2}$ as compared to the Pt NP coated GCE ($2.7 \times 10^{-4}$ A $cm^{-2}$) or the

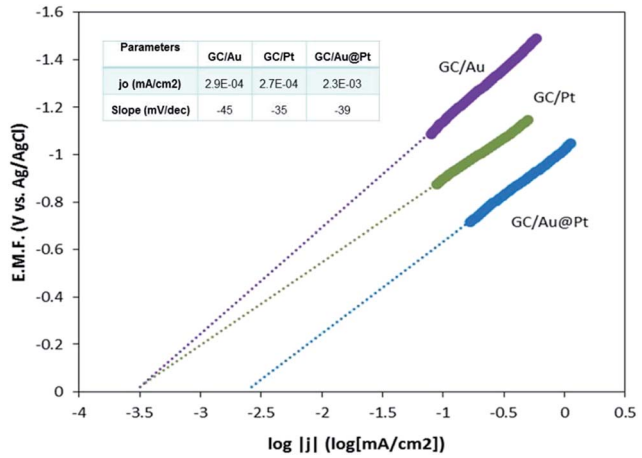


Fig. 8 Tafel slopes for the hydrogen evolution reaction on Au NPs, Pt NPs and Au@Pt NPs (inset: table showing data extracted from Tafel plot).

Au NP coated GCE ($2.9 \times 10^{-4}$ A $cm^{-2}$), resulting in a lower activation energy. Our results are comparable with other similar studies in terms of the Tafel slope values obtained (Pt), ranging from 75 to 125 mV $decade^{-1}$.[41] However, the resulting exchange current density for our system is two decades lower as compared with other polycrystalline Pt catalyst in alkaline medium.[42]

The improved HER of Au@Pt NPs compared with pure Pt catalyst can be attributed to the presence of gold that oxidizes the adsorbed species on the active sites of platinum nanoparticles, thereby improving the catalytic activity of Au@Pt NPs. In addition, these hybrid nanospheres have Pt sponge-like structure (porosity), which increases the efficient surface-to-volume ratios and utilization efficiency of Pt.

On-going work is focused on a better understanding of the high electrocatalytic activity displayed by Trp mediated synthesis of Au@Pt NPs as several improved catalytically active nanostructures could be synthesized using this green chemistry approach. We found our Trp mediated core–shell nanoparticle technique to be highly flexible for the synthesis of a range of nanoparticles including Au@Pt, Au@Pd, Au@Ag, Au@Rh (ESI†). These nanoparticles could be exploited in heterogeneous catalysis for clean energy, organic synthesis and water remediation amongst a plethora of further applications.

## Conclusion

We have presented a facile one-pot green synthesis of Au@Pt bimetallic NPs with a core–shell structure. We observed octahedronal gold forming the core (~50 nm) with a Pt layer (~5 nm) forming the shell. We elucidated that the thickness of the Pt layer is time dependent, keeping the other reaction parameters constant. The resulting Au@Pt NPs were characterized using TEM, AC-HAADF-STEM, STEM-EDX, XRD and CV to confirm and analyze the resulting composition of core–shell morphology. The work reported here demonstrates for the first time, the synthesis of stable Au@Pt bimetallic nanoparticles (core–shell type) by successive reduction in the presence of an amino acid (Trp), at room temperature. Finally, the catalytic activity of these nanoparticles was evaluated for HER by depositing them over a GCE and the Au@Pt NPs were observed to have the highest HER potential with the lowest required applied potential, demonstrating them to be ideal candidates as catalysts for the fabrication of HER oriented electrodes. Trp mediated synthesis promises to be a cost-effective bulk synthesis strategy for the production of a diverse range of multi-layered nanostructures including core–shell nanoparticles.

## Acknowledgements

We would like to extend our sincere gratitude to Dr Minoru Mizuhata for facilitating XPS analysis. This work was partly supported by Special Coordination Fund for Promoting Science and Technology, Creation of Innovative Centers for Advanced Interdisciplinary Research Areas (Innovative Bioproduction Kobe) from the Ministry of Education, Culture, Sports and Technology (MEXT) and partly by the MEXT Scholarship research fund.

## Notes and references

1 N. Toshima and T. Yonezawa, *New J. Chem.*, 1998, **22**, 1179.
2 R. W. J. Scott, O. M. Wilson, S. K. Oh, E. A. Kenik and R. M. Crooks, *J. Am. Chem. Soc.*, 2004, **126**, 15583.
3 J. Luo, P. N. Njoki, Y. Lin, D. Mott, L. Wang and C. J. Zhong, *Langmuir*, 2006, **22**, 2892.
4 W. Tang, S. Jayaraman, T. F. Jaramillo, G. D. Stucky and E. W. McFarland, *J. Phys. Chem. C*, 2009, **113**, 5014.
5 A. Sarkar and A. Manthiram, *J. Phys. Chem. C*, 2010, **114**, 4725.
6 K. Sasaki, H. Naohara, Y. Cai, Y. M. Choi, P. Liu, M. B. Vukmirovic, J. X. Wang and R. R. Adzic, *Angew. Chem., Int. Ed.*, 2010, **49**, 8602.
7 D. F. Yancey, E. V. Carino and R. M. Crooks, *J. Am. Chem. Soc.*, 2010, **132**, 10988.
8 H. A. Esfahani, L. Wang and Y. Yamauchi, *Chem. Commun.*, 2010, **46**, 3684.
9 S. K. Srivastava, R. Yamada, C. Ogino and A. Kondo, *Nanoscale Res. Lett.*, 2013, **8**, 70.
10 S. K. Srivastava, R. Yamada, C. Ogino and A. Kondo, *Carbon*, 2013, **56**, 309.
11 B. Wickleinab and G. S. Alvarez, *J. Mater. Chem. A*, 2013, **1**, 5469.
12 D. J. Chen, A. M. H. Duffy, I. S. Park, D. O. Atienza, C. Susut, S. G. Sun and Y. J. Tong, *J. Phys. Chem. C*, 2011, **115**, 8735.
13 J. Zhang, F. H. B. Lima, M. H. Shao, K. Sasaki, J. X. Wang, J. Hanson and R. R. Adzic, *J. Phys. Chem. B*, 2005, **109**, 22701.
14 S. K. Srivastava and M. Constanti, *J. Nanopart. Res.*, 2012, **14**, 831.
15 G. Clergeaud, R. Genç, M. Ortiz and C. K. O'Sullivan, *Langmuir*, 2013, **29**, 15405.
16 S. K. Srivastava, R. Yamada, C. Ogino and A. Kondo, *RSC Adv.*, 2014, **4**, 5986.
17 O. V. Kharissova, H. V. Dias, B. I. Kharisov, B. O. Pérez and V. M. Pérez, *Trends Biotechnol.*, 2013, **31**, 240.

18 X. Liu, J. Zhang, X. Guo, S. Wu and S. Wang, *Nanoscale*, 2010, **2**, 1178.
19 R. R. Naik, S. J. Stringer, G. Agarwal, S. E. Jones and M. O. Stone, *Nat. Mater.*, 2002, **1**, 169.
20 S. K. Srivastava, T. Hasegawa, R. Yamada, C. Ogino, M. Mizuhata and A. Kondo, *RSC Adv.*, 2013, **3**, 18367.
21 P. R. Selvakannan, S. Mandal, S. Phadtare, A. Gole, R. Pasricha and S. D. Adyanthaya, *J. Colloid Interface Sci.*, 2004, **269**, 97.
22 M. Iosin, P. Baldeck and S. Astilean, *J. Nanopart. Res.*, 2010, **12**, 2843.
23 Y. Hou, T. Huang, Z. Wen, S. Mao, S. Cui and J. Chen, *Adv. Energy Mater.*, 2014, **4**, DOI: 10.1002/aenm.201400337.
24 S. A. Grigoriev, P. Millet and V. N. Fateev, *J. Power Sources*, 2008, **177**, 281.
25 E. Ndzebet and O. Savadogo, *Int. J. Hydrogen Energy*, 1995, **20**, 635.
26 J. D. Newman and G. J. Blanchard, *Langmuir*, 2006, **22**, 5882.
27 S. Si and T. K. Mandal, *Chem.–Eur. J.*, 2007, **13**, 3160.
28 J. H. Song, F. Kim, D. Kim and P. D. Yang, *Chem.–Eur. J.*, 2005, **11**, 910.
29 J. W. Hu, Y. Zhang, H. V. Li, Z. Liu, B. Ren, S. G. Sun, Z. Q. Tian and T. Lian, *Chem. Phys. Lett.*, 2005, **408**, 354.
30 K. Y. Lee, M. Kim, Y. W. Lee, J. J. Lee and S. W. Han, *Chem. Phys. Lett.*, 2007, **440**, 249.
31 Y. Hayakawa, A. Kawashima, H. Habazaki, K. Asami and K. Hashimoto, *J. Appl. Electrochem.*, 1992, **22**, 1017.
32 M. Tejos, R. Schrebler, F. R. Díaz and M. A. del Valle, *Thin Solid Films*, 2002, **409**, 172.
33 Y. W. Lee, M. Kim, Z. H. Kim and S. W. Han, *J. Am. Chem. Soc.*, 2009, **131**, 17036.
34 M. R. Gao, X. Cao, Q. Gao, Y. F. Xu, Y. R. Zheng, J. Jiang and S. H. Yu, *ACS Nano*, 2014, **8**, 3970.
35 M. H. Abd Elhamid, B. G. Ateya, K. G. Weil and H. W. Pickering, *J. Electrochem. Soc.*, 2000, **147**, 2148.
36 M. N. Desic, M. M. Popovic, M. D. Obradovic, L. M. Vracar and B. N. Grgur, *J. Serb. Chem. Soc.*, 2005, **70**, 231.
37 G. Kokkinidis, A. Papoutsis, D. Stoychevb and A. Milchev, *J. Electroanal. Chem.*, 2000, **486**, 48.
38 A. Kiani and S. Hatami, *Int. J. Hydrogen Energy*, 2010, **35**, 5202.
39 E. R. Tourwé, R. Pintelon and A. Hubin, *J. Electroanal. Chem.*, 2006, **594**, 50.
40 N. M. Markovica, S. T. Sarraf, H. A. Gasteiger and P. N. Ross, Hydrogen electrochemistry on platinum low-index single-crystal surfaces in alkaline solution, *J. Chem. Soc., Faraday Trans.*, 1996, **92**, 3719–3725.
41 B. E. Conway and L. Bai, *J. Chem. Soc., Faraday Trans. 1*, 1985, **81**, 1841.
42 V. S. Bagotzky and V. Osterova, *J. Electroanal. Chem.*, 1973, **43**, 233.